JCARME
ISSN: 2228-7922
Journal of Computational and Applied Research in Mechanical Engineering
Vol. 9, No. 2, pp. 275-285
jcarme.sru.ac.ir

Magneto Prandtl nanofluid past a stretching surface with non-linear radiation and chemical reaction

K. Ganesh Kumar [a], G. K. Ramesh [b, *], S. A. Shehzad [c] and B. J. Gireesha [d]

[a]Department of Mathematics, S.J.M. Institute of Technology, Chitradurga-577501, Karnataka, India
[b]Department of Mathematics, K.L.E Society's J.T. College, Gadag-582102, Karnataka, India
[c]Department of Mathematics, COMSATS Institute of Information Technology, Sahiwal 57000, Pakistan
[d]Department of Studies and Research in Mathematics, Kuvempu University, Shankaraghatta-577 451, Shimoga, Karnataka, India

Article info:
Type: Research
Received: 20/12/2017
Revised: 31/10/2018
Accepted: 02/11/2018
Online: 04/11/2018

Keywords:
MHD flow,
Prandtl nanofluid,
Nonlinear thermal radiation,
chemical reaction,
slip effect.

Abstract

In this article, we examined the behavior of chemical reaction effect on a magnetohydrodynamic Prandtl nanofluid flow due to stretchable sheet. Non-linear thermally radiative term is accounted in energy equation. Constructive transformation is adopted to formulate the ordinary coupled differential equations system. This system of equations is treated numerically through Runge Kutta Fehlberg-45 method based shooing method. The role of physical constraints on liquid velocity, temperature and concentration are discussed through numerical data and plots. Also, the skin friction co-efficient, local Nusselt number and local Sherwood numbers are calculated to study the flow behavior at the wall, which is also presented in tabular form. A comparative analysis is presented with the previous published data in special case for the justification of the present results. The output reveals that for larger values of elastic and Prandtl parameter, the thickness of momentum layer enhanced and the rates of both heat and mass transport reduced. Also, increment of slip parameter decelerated both temperature and concentration filed while nonlinear form thermal radiation rapidly increases the temperature.

Nomenclature

A and c	Material constants
b	Constant
B_0	Magnetic field
B	Thermal slip parameter
C	Nanoparticle volume fraction
C_w	Concentration at wall
C_∞	Ambient nanofluid volume fraction
C_{fx}	Skin friction coefficient
c_p	Specific heat coefficient
D	Solutal slip parameter
D_B	Coefficient of Brownian diffusion
D_T	Coefficient of thermophoretic diffusion
K	Chemical reaction coefficient
K_1 and K_2	Slip factor
k	Thermal conductivity
k^*	Mean absorption coefficient
Le	Lewis number
Nb	Brownian motion parameter

*Corresponding author
Email address: gkrmaths@gmail.com

Nt	Thermophoresis parameter
Nu_x	Local Nusselt number
Pr	Prandtl number
q_r	Radiative heat flux
q_w	Heat flux
q_m	Mass flux
Ra	Radiation parameter
Re_x	Local Reynolds number
Sh_x	Local Sherwood number
T	Fluid temperature
T_w	Surface temperature
T_∞	Ambient surface temperature
u, v	Velocity components
U_w	Stretching sheet
x, y	Coordinates

Greek symbols

θ	Dimensionless temperature
θ_w	Temperature ratio parameter
ϕ	Dimensionless nanoparticle volume fraction
ν	Kinematic viscosity of the fluid
β	Volumetric coefficient
μ	Dynamic viscosity
σ^*	Stefan–Boltzmann constant
τ	Ratio of effective heat capacity of nanoparticle to ordinary liquid
τ_w	Shear stress along the wall
α	Prandtl parameter
β	Elastic parameter
α_1	Liquid thermal diffusivity
λ	Mixed convection parameter
γ	Chemical reaction parameter
ρ	Density of the fluid

1. Introduction

Significant attention has been given in the recent years to address the behavior of flow and heat analysis on nanofluids. The reason is ordinary fluids having the low thermal conductivity. By adding the nano size particles in an ordinary fluid, thermal conductivity of liquid enhanced dramatically as was examined by Chio [1]. Comprehensive detail of convective transport in nanofluid has been investigated by Buongiorno [2]. Khan and Pop [3] analyzed the thermoporesis and Brownian mothion effects on boundary layer flow due to stretching surface. Makinde et al [4] examined the heat transport behavior in nanofluid flow past a convective type heating surface. Sheikholeslami et al [5] provided numerical solution for Magneto nanofluid flow and heat transfer characteristics in a rotating framework. Ramesh et al [6-8] studied the two and three dimensional flow of non-newtonian nanofluid over a different geometry.

Nowadays, many researchers are concentrating on the exploration of non-Newtonian liquids, because non-Newtonian fluids have multidisciplinary applications in modern industrial and technological products. Few examples of non-Newtonian materials include food, ketchup, shampoos, slurries, granular suspension, paper pulp, paints, polymer solutions, certain oils, and clay coatings. All features of non-Newtonian liquids cannot be distinguished by a single mathematical relationship. Govardhan et al. [9] initiated that the magnetohydrodynamics effects in mixed convective micropolar liquid over moving sheet. Cortell [10] discussed the hydromagnetic power-law liquid flow. Malik et al. [11] employed Keller box technique to study tangent hyperbolic liquid flow under magnetic force induced by moving cylinder. Rehena et al. [12] investigated the Prandtl number effect on assisted convective heat transfer through a solar collector. Akbar at al. [13] studied the magnetohydrodynamic tangent hyperbolic liquid flow towards a stretched sheet with magnetic field. Nasrin and Alim [14] analyzed the Prandtl number effect on free convective flow in a solar collector utilizing nanofluid. Nadeem et al. [15] addressed the importance of stenosis and nanoparticle in peristaltic Prandtl fluid flow.

Thermal radiation has a potential role in manufacturing design of nuclear power plants and various engineering processes. Numerous researchers have paid their attention to address the mechanism of thermal radiation. Shehzad et al. [16] reported nonlinear radiation in three dimensional Jeffrey nanofluid flow induced by the bi-directionally moving surface. Influence of nonlinear thermal radiation on Carreau nanofluid over a nonlinear form of stretched sheet is reported by Zaib et al. [17]. The recent advancements in phenomenon of nonlinear radiation heat transport have been demonstrated in the studies [18-22]. The role of slip and thermal jump conditions on heat transport for both Newtonian and non-Newtonian liquid sunder various flow geometries has been reported by various researchers. Wang [23] discussed the partial slip boundary conditions over moving stretched sheet. The effect of slip exponentially boundary layer stretched flow with thermal radiation has been described by Swati and Gorla [24]. Fang et al [25] performed the flow past a shrinking sheet by considering second order slip. Bhattacharyya et al [26] explored the slip effects on free stream velocity across a shrinking sheet. Das et al [27] addressed the heat source/sink effect on nanofluid flow in a vertical direction. Kezzar et al. [28] obtained the series solution for flow over a stretchable/shrinkable wall in the presence of nanoparticles. Further Kezzar et al. [29] discussed the heat transport performance on magneto nanofluid flow in a non-parallel plate.

Gaining motivation from the above studies, we want to analyze the importance of chemical reaction and multiple slip effects on Prandtl nanofluid flow past a stretchable surface. In addition, the effect of transverse magnetic field and nonlinear thermal radiation are included. Using suitable similarity variables, the governed partial differential systems are converted into system of non-linear ordinary differential equations and then tackled numerically. The numerical values of the skin friction coefficient and local Nusselt number are also recorded in a tabular form.

2. Mathematical analysis

We considered the steady-state incompressible Prandtl nanoliquid flow over a stretchable sheet. The x-axis is along the sheet and y-axis normal to it. Here the flow generation is due to linear stretching of surface with distance x, i.e. $U_w = bx$. A constant magnetic field with strength B_0 is implemented in transverse flow direction. T_w is the surface temperature at wall and C_w the solutal concentration. At larger distance from surface, temperature and nanoparticle concentration is represented by T_∞ and C_∞ respectively.

The continuity, momentum, energy and concentration expressions are described as (See Akbar et al [13])

$$\frac{\partial u}{\partial x} + \frac{\partial v}{\partial y} = 0, \tag{1}$$

$$u\frac{\partial u}{\partial x} + v\frac{\partial u}{\partial y} = \nu\frac{\mathrm{A}}{\mathrm{c}}\frac{\partial^2 u}{\partial y^2} + \frac{\nu A}{2c^3}\left(\frac{\partial u}{\partial y}\right)^2\frac{\partial^2 u}{\partial y^2} - \frac{\sigma B_0^2}{\rho}u, \tag{2}$$

$$u\frac{\partial T}{\partial x} + v\frac{\partial T}{\partial y} = \alpha_1\frac{\partial^2 T}{\partial y^2} + \tau\left[D_B\frac{\partial C}{\partial y}\frac{\partial T}{\partial y} + \frac{D_T}{T_\infty}\left(\frac{\partial T}{\partial y}\right)^2\right] - \frac{\partial q_r}{\partial y}, \tag{3}$$

$$u\frac{\partial C}{\partial x} + v\frac{\partial C}{\partial y} = D_B\frac{\partial^2 C}{\partial y^2} + \frac{D_T}{T_\infty}\frac{\partial^2 T}{\partial y^2} + K(C - C_\infty), \tag{4}$$

with the relevant boundary conditions

$$u = u_w,\ \ v = 0,\ \ T = T_w + K_1\frac{\partial T}{\partial y},$$
$$C = C_w + K_2\frac{\partial C}{\partial y}\ \text{ at } y = 0,$$
$$u \to 0,\ \ T \to T_\infty,\ \ C \to C_\infty \text{ as } y \to \infty, \tag{5}$$

here the velocity components are presented by u and v, α_1 for thermal diffusivity, $\nu = \frac{\mu}{\rho}$ for kinematic viscosity, β for coefficient volumetric thermal expansion, ρ for liquid density, σ for electrical conductivity, A and c for material constants of Prandtl fluid model, τ for nanoparticle effective heat capacity of the liquid, K for chemical reaction coefficient, K_1 and K_2 are thermal and concentration slip factor, D_B for Brownian diffusion coefficient and D_T for thermophoresis diffusion coefficient, T for fluid temperature, C for nanoparticle volume friction, q_r for radiative heat flux.

Radiation heat flux q_r via Rosseland approximation can be set in the form(See Zaib et al [17]):

$$q_r = -\frac{4\sigma^*}{3k^*}\frac{\partial T^4}{\partial y} = -\frac{16\sigma^*}{3k^*}T^3\frac{\partial T}{\partial y}, \tag{6}$$

where σ^* for Stefan–Boltzmann constant and k^* for coefficient of mean absorption.

The law of energy with radiation heat flux takes the form

$$u\frac{\partial T}{\partial x}+v\frac{\partial T}{\partial y}=\frac{\partial}{\partial y}\left[\left(\alpha_1+\frac{16\sigma^* T^3}{3k^*}\right)\frac{\partial T}{\partial y}\right]+\tau\left[D_B\frac{\partial c}{\partial y}\frac{\partial T}{\partial y}+\frac{D_T}{T_\infty}\left(\frac{\partial T}{\partial y}\right)^2\right]. \quad (7)$$

For the mathematical analysis of problem, we use the following transformation (see Ramesh [6])

$$u=bxf'(\eta), v=-\sqrt{bv}\,f(\eta),\ \eta=\sqrt{\frac{b}{v}}y,$$
$$T=T_\infty(1+(\theta_w-1)\theta(\eta)),\quad \phi(\eta)=\frac{C-C_\infty}{C_w-C_\infty}, \quad (8)$$

where $\theta_w=\frac{T_w}{T_\infty},\ \theta_w>1$ being the temperature ratio parameter.

After utilizing Eq. (8), Eq. (1) is identically satisfied and Eqs. (2, 4 and 7) take the following form

$$\alpha f'''(\eta)-[f'(\eta)]^2+f''(\eta)f(\eta)+\beta f''^2(\eta)f'''(\eta)-Mf'(\eta)=0, \quad (9)$$

$$\left(\left(1+\frac{4}{3}Ra\left(1+(\theta_w-1)\theta(\eta)\right)^3\right)\theta'(\eta)\right)'+\Pr\left(f(\eta)\theta'(\eta)+Nb\theta'(\eta)\phi'(\eta)+Nt\,\theta'^2(\eta)\right), \quad (10)$$

$$\phi''(\eta)++Le\,f(\eta)\,\phi'(\eta)+\frac{Nt}{Nb}\theta''(\eta)-\gamma\phi'(\eta)=0, \quad (11)$$

with the boundary conditions

$$f(\eta)=0,\ f'(\eta)=1,\theta(\eta)=1+B\theta'(\eta),\ \phi(\eta)=1+D\phi'(\eta)\text{ at }\eta=0,$$
$$f'(\eta)=0,\ \theta(\eta)\to 0,\ \phi(\eta)\to 0\ \text{ as }\ \eta=\infty, \quad (12)$$

where $M=\frac{\sigma B_0^2}{\rho b}$ for magnetic parameter, $\alpha=\frac{1}{\mu Ac}$ for Prandtl parameter, $\beta=\frac{bU_w}{2c^2v}$ for elastic parameter, $Pr=\frac{v}{\alpha_1}$ for Prandtl number, $Ra=\frac{4\sigma^* T_\infty^3}{kk^*}$ for radiation parameter, $Le=\frac{v}{D_B}$ for Lewis number, $Nb=\frac{\tau D_B(C_w-C_\infty)}{v}$ for Brownian motion parameter, $Nt=\frac{\tau D_T(T_w-T_\infty)}{T_\infty v}$ for thermophoresis parameter, $\gamma=\frac{KU_w(C-C_\infty)}{v}$ for chemical reaction parameter, $B=K_1\sqrt{\frac{b}{v}}$ for thermal slip parameter and $D=K_2\sqrt{\frac{b}{v}}$ for solutal slip parameter.

The physical quantities of interest likes skin friction coefficient$\left(C_{fx}\right)$ local Nusselt number (Nu_x) and local Sherwood number (Sh_x) are defined as:

$$c_{fx}=\frac{\tau_w}{\rho U_w^2}, Nu_x=\frac{u_w q_w}{ka(T_w-T_\infty)}\text{ and } Sh_x=\frac{u_w q_m}{aD_b(C_w-C_\infty)}, \quad (13)$$

where τ_w is known as shear stress along the wall, q_w is known as heat flux, q_m is nanoparticle mass flux,

$$\tau_w=\frac{A}{c}\frac{\partial u}{\partial y}+\frac{A}{2c^3}\left(\frac{\partial u}{\partial y}\right)^3,\quad q_w=-k\frac{\partial T}{\partial y}|_{y=0}\text{ and } q_m=-D\frac{\partial C}{\partial y}|_{y=0}. \quad (14)$$

Dimensionless form of local skin friction coefficient (C_{fx}), local Nusselt number (Nu_x) and local Sherwood number (Sh_x) are

$$\sqrt{Re}C_{fx}=[\alpha f''(\eta)+\beta f''(\eta)^3]_{\eta=0},\ \frac{Nu_x}{Re^{\frac{1}{2}}}=-\left[1+\frac{4}{3}Ra\,\theta_w^3\right]\theta'(0), \frac{Sh_x}{Re^{\frac{1}{2}}}=-\phi'(0), \quad (15)$$

where the local Reynolds number $Re_x=\frac{U_w(x)}{av}$.

3. Numerical solutions

Numerical scheme of non-linear differential Eqs. (9-11) with conditions (12) correspond to two-point boundary value problem. The solutions in closed form cannot be constructed due to high non-linearity and coupled nature of govern system. Therefore, we developed the numerical results. We adopted the most effective fourth-fifth order Runge-Kutta-Fehlberg method through shooting procedure. The selection of suitable finite range of η_∞ is the most valuable part of this scheme. Tables 1 and 2 are constructed for the comparative study of the present results with those of previous ones for various values of c and show a good agreement with each other.

4. Results and discussion

This section deals with the impact of various physical constraints on velocity $f'(\eta)$, temperature $\theta(\eta)$ and concentration $\phi(\eta)$. Fig. 1 illustrates the variation of Prandtl parameter (α) on $f'(\eta)$, $\theta(\eta)$ and $\phi(\eta)$. As the value of Prandtl fluid parameter raised, the velocity of liquid and corresponding boundary layer increases. This happens because by increasing the Prandtl fluid parameter, the viscosity of fluid decreases. Consequently, fluid becomes less viscous for higher values of Prandtl fluid and velocity profiles increase. Further, it was revealed that both $\theta(\eta)$ and $\phi(\eta)$ and their associated thickness of boundary layers decrease with an increment Prandtl parameter.

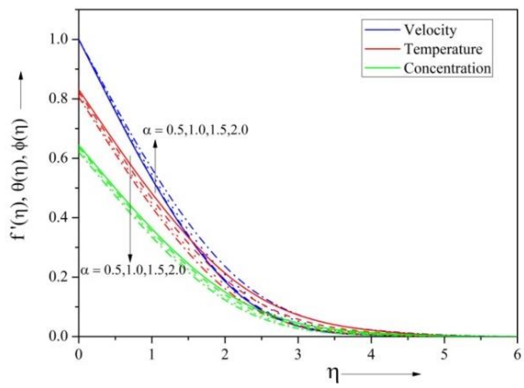

Fig. 1. Impact of α on $f'(\eta)$, $\theta(\eta)$ and $\phi(\eta)$.

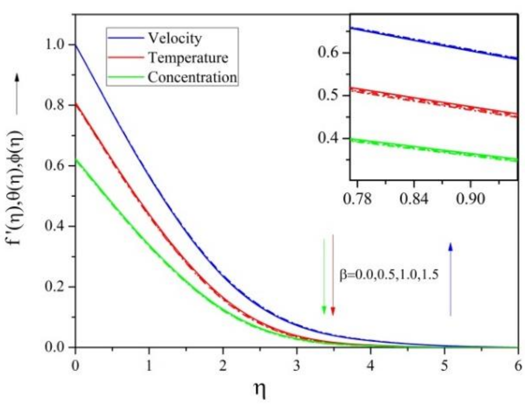

Fig. 2. Impact of β on $f'(\eta)$, $\theta(\eta)$ and $\phi(\eta)$.

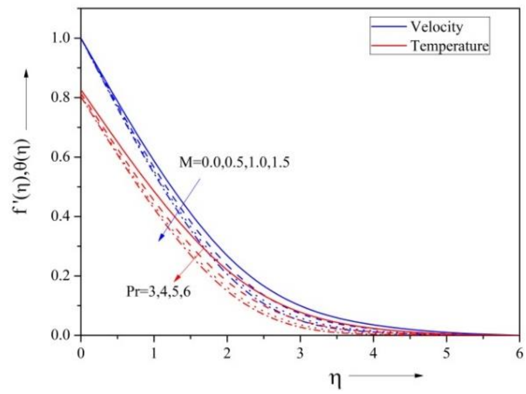

Fig. 3. Impact of M on $f'(\eta)$ and Pr on $\theta(\eta)$.

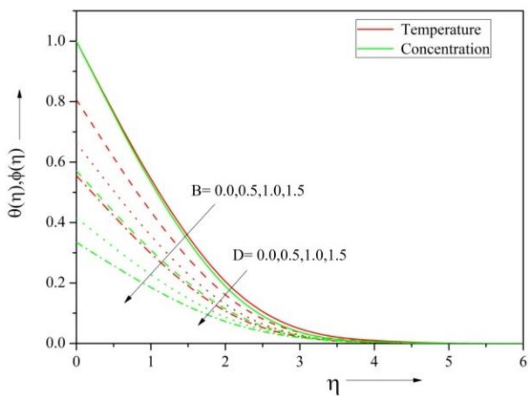

Fig. 4. Impact of B on $\theta(\eta)$ and D on $\phi(\eta)$.

Variations of elastic parameter (β) on $f'(\eta)$, $\theta(\eta)$ and $\phi(\eta)$ are depicted in Fig. 2. It is revealed that a reduction is occurred in the $f'^{(\eta)}$ when the values of elastic parameter enhance. This type of behavior is validated because by increasing β viscosity increases which as an outcome gears down the velocity. But the opposite behavior can be seen in temperature and concentration profile.

Fig. 3 shows the importance of magnetic parameter (M) on $f'(\eta)$ and Prandtl number(Pr) on $\theta(\eta)$. It is concluded that higher values of M lead to lower velocity. The reason is the potentiality of Lorentz force which takes place due to the magnetic field. This force restricts the flow intensity. Also, in Fig. 3, we demonstrate the effect of (Pr) on $\theta(\eta)$. It is noted that larger Prandtl number reduced the temperature.

Fig. 4 illustrates the effect of thermal slip parameter (B) on $\theta(\eta)$. We can observe that the increasing value of thermal slip parameter reduces the thickness of thermal boundary layer and hence decreases the temperature. The coefficient of thermal accommodation is enhanced due to larger thermal slip parameter, as a result of which a decrement is noticed in thermal efficiency towards the flow. Further, Fig. 4 is sketched to reveal the effects of solutal slip parameter (D) on $\phi(\eta)$. This plot clearly demonstrates that $\phi(\eta)$ decreases with increasing solutal slip parameter.

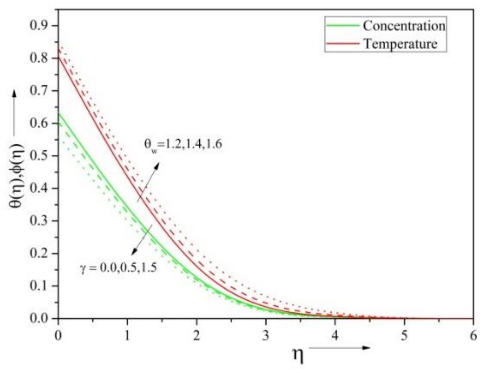

Fig. 5. Impact of θ_w on $\theta(\eta)$ and γ on $\phi(\eta)$.

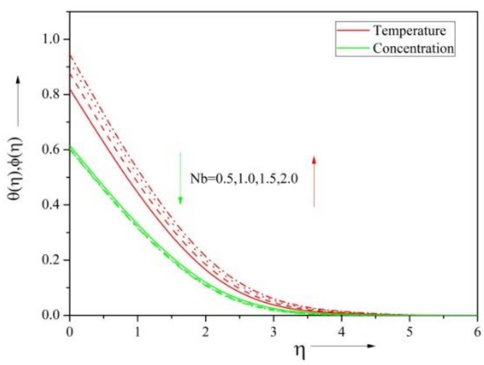

Fig. 6. Impact of Nb on $\theta(\eta)$ and $\phi(\eta)$.

Fig. 5 delineates the variations of $\theta(\eta)$ versus η for various values of temperature ratio parameter (θ_w). We have visualized that an increase in θ_w enhances $\theta(\eta)$ and its associated layer thickness. The behavior of chemically reactive parameter(γ) on $\phi(\eta)$ is observed in Fig. 5. We visualized that $\phi(\eta)$ and thickness of associated layer are decreasing while increase of γ. For the features of nanoparticle volume mechanism, the nanoparticle volume field higher distortion is caused at $\gamma = 1.0$.

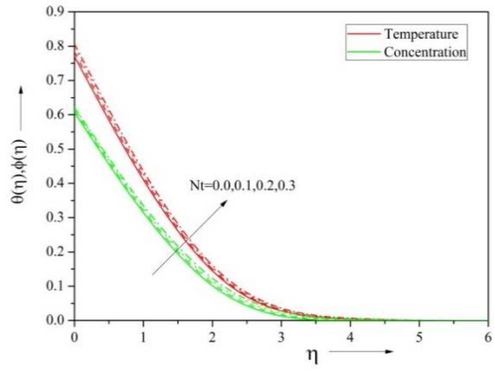

Fig. 7. Impact of Nt on $\theta(\eta)$ and $\phi(\eta)$.

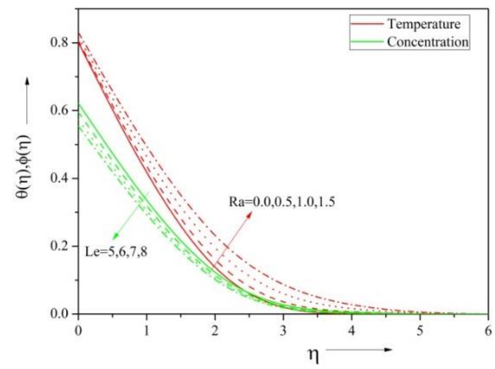

Fig. 8. Impact of Ra on $\theta(\eta)$ and Le on $\phi(\eta)$.

Fig. 6 portraits the effect of Brownian movement parameter (Nb) on $\theta(\eta)$ and $\phi(\eta)$. The temperature curves are higher for larger Brownian movement. As Nb increases, random motion of liquid particles increased that corresponds to more heat production. Thus, temperature profiles show increasing behavior whereas the concentration profiles show opposite behavior. The impacts of thermophoresis parameter (Nt) on $\theta(\eta)$ and $\phi(\eta)$ are depicted in Fig. 7. From this plot, it can be examined that larger thermophoretic parameter is to increase $\theta(\eta)$ and $\phi(\eta)$.

Fig. 8 explains the characteristic of radiative parameter(Ra) on $\theta(\eta)$. The higher radiative parameter gives an enhancement to temperature. More heat is generated in liquid due to radiation phenomenon that results in larger temperature. Further, Fig. 8 elucidates that $\phi(\eta)$ decreases as Lewis number increases. The physical argument behind this is that the increase in Lewis number implies decrease in solute diffusivity which consequently reduces concentration profile and mass transfer rate.

Table 1. Comparison table of skin friction coefficient($\alpha = \beta = 0$).

M	Akbar et al [13] (RKF method)	Cortell [10] (RK algorithm)	Present results (RKF-45 method)	Errors
1	-1.41421	-1.414	-1.41421	0.00000
5	-2.44948	-2.449	-2.44949	0.00001
10	-3.31662	-3.316	-3.31662	0.00000
50	-7.14142	-7.141	-7.14143	0.00001
500	-22.3830	-22.383	-22.38302	0.00002
1000	-31.6386	-31.638	-31.63858	0.00002

Table 2. Comparison of the result for Nusselt number $-\theta\,'(0)$.

$\boldsymbol{Pr}$	Khan and Pop [3]	Wang [30]	Gorla and Sidawi [31]	Present result (RKF-45 method)	Errors
0.7	0.4539	0.4539	0.5349	0.45357	-0.00033
2	0.9113	0.9114	0.9114	0.91135	0.00005
7	1.8954	1.8954	1.8905	1.89539	-0.00001
20	3.3539	3.3539	3.3539	3.35387	-0.00003
70	6.4621	6.4622	6.4622	6.46209	-0.00001

Table 3. Variation of skin friction coefficient, Nusselt number and Sherwood number for different physical parameter.

B	D	θ_w	γ	Le	M	Nb	Nt	Pr	Ra	α	β	$\sqrt{\boldsymbol{Re_x}}\boldsymbol{C_f}$	$-\frac{\boldsymbol{Sh_x}}{\sqrt{\boldsymbol{Re_x}}}$	$-\frac{\boldsymbol{Nu_x}}{\sqrt{\boldsymbol{Re_x}}}$
0	0.4	1.2	0.2	0.5	0.5	0.4	0.3	5	0.5	1	0.6	0.425488	0.947083	0.190698
0.5												0.409816	0.946238	0.124681
1												0.39773	0.946853	0.082593
0.3	0	1.2	0.2	0.5	0.5	0.4	0.3	5	0.5	1	0.6	0.419743	1.604065	0.081839
	0.5											0.415039	0.858037	0.15961
	1											0.413154	0.584691	0.202559
0.3	0.4	1.2	0.2	0.5	0.5	0.4	0.3	5	0.5	1	0.6	0.41563	0.946352	0.147669
		1.4										0.422245	0.956955	0.124959
		1.6										0.428982	0.965989	0.102936
0.3	0.4	1.2	0	0.5	0.5	0.4	0.3	5	0.5	1	0.6	0.415775	0.915744	0.146925
			0.5									0.415432	0.987935	0.148739
			1									0.415145	1.047913	0.150419
0.3	0.4	1.2	0.2	5	0.5	0.4	0.3	5	0.5	1	0.6	0.41563	0.946352	0.147669
				6								0.415392	1.011447	0.146891
				7								0.415156	1.06673	0.146968
0.3	0.4	1.2	0.2	0.5	0	0.4	0.3	5	0.5	1	0.6	0.49145	0.964897	0.166639
					0.5							0.41563	0.946352	0.147669
					1							0.284219	0.931216	0.133163
0.3	0.4	1.2	0.2	0.5	0.5	0.5	0.3	5	0.5	1	0.6	0.417295	0.962536	0.117544
						1						0.424469	0.990976	0.036334
						1.5						0.42999	0.997023	0.01069
0.3	0.4	1.2	0.2	0.5	0.5	0.4	0	5	0.5	1	0.6	0.408612	0.983517	0.264953
							0.1					0.411021	0.965947	0.217232
							0.2					0.413361	0.953892	0.178757
0.3	0.4	1.2	0.2	0.5	0.5	0.4	0.3	3	0.5	1	0.6	0.425187	0.948021	0.104965
								4				0.419522	0.945832	0.13088
								5				0.41563	0.946352	0.147669
0.3	0.4	1.2	0.2	0.5	0.5	0.4	0.3	5	0	1	0.6	0.408766	0.957383	0.074559
									0.5			0.41563	0.946352	0.147669
									1			0.421678	0.946355	0.185743
0.3	0.4	1.2	0.2	0.5	0.5	0.4	0.3	5	0.5	0.5	0.6	-0.34501	0.921984	0.124896
										1		0.41563	0.946352	0.147669
										1.5		0.907859	0.961428	0.162777
0.3	0.4	1.2	0.2	0.5	0.5	0.4	0.3	5	0.5	1	0	1.099521	0.939479	0.140804
											0.5	0.502964	0.945404	0.146706
											1	0.121264	0.949664	0.15107

Table 4. Values of Nusselt number for different values of the physical parameters when linear and nonlinear radiation.

B	D	γ	Le	M	Nb	Nt	Pr	Ra	α	β	Linear $-\frac{Nu_x}{\sqrt{Re_x}}$	Nonlinear $-\frac{Nu_x}{\sqrt{Re_x}}$
0	0.4	0.2	0.5	0.5	0.4	0.3	5	0.5	1	0.6	0.138803	0.190698
0.5											0.081143	0.124681
1											0.049296	0.082593
0.3	0	0.2	0.5	0.5	0.4	0.3	5	0.5	1	0.6	0.043111	0.081839
	0.5										0.111325	0.15961
	1										0.152135	0.202559
0.3	0.4	0	0.5	0.5	0.4	0.3	5	0.5	1	0.6	0.099968	0.147669
		0.5									0.100638	0.124959
		1									0.101362	0.102936
0.3	0.4	0.5	5	0.5	0.4	0.3	5	0.5	1	0.6	0.100228	0.146925
			6								0.098082	0.148739
			7								0.096989	0.150419
0.3	0.4	0.5	0.5	0	0.4	0.3	5	0.5	1	0.6	0.11126	0.147669
				0.5							0.100228	0.146891
				1							0.091731	0.146968
0.3	0.4	0.2	0.5	0.5	0.5	0.3	5	0.5	1	0.6	0.072937	0.166639
					1						0.012659	0.147669
					1.5						0.001745	0.133163
0.3	0.4	0.2	0.5	0.5	0.4	0	5	0.5	1	0.6	0.212693	0.117544
						0.1					0.165202	0.036334
						0.2					0.128514	0.01069
0.3	0.4	0.2	0.5	0.5	0.4	0.3	3	0.5	1	0.6	0.086392	0.264953
							4				0.097146	0.217232
							5				0.100228	0.178757
0.3	0.4	0.2	0.5	0.5	0.4	0.3	5	0	1	0.6	0.084669	0.104965
								0.5			0.100228	0.13088
								1			0.093664	0.147669
0.3	0.4	0.2	0.5	0.5	0.4	0.3	5	0.5	0.5	0.6	0.086621	0.074559
									1		0.100228	0.147669
									1.5		0.109125	0.185743
0.3	0.4	0.2	0.5	0.5	0.4	0.3	5	0.5	1	0	0.095756	0.124896
										0.5	0.09961	0.147669
										1	0.102389	0.162777

Variations of skin friction coefficient, Nusselt and Sherwood numbers for various values of flow controlling parameters are reported numerically in Table 3. This table is evident to show that the skin friction coefficient increases by increasing temperature ratio, Brownian movement, thermophoretic, radiation, elastic and Prandtl parameters. The higher values of thermal slip, solutal slip, chemical reaction, Lewis number and magnetic parameter caused a decrement in skin friction coefficient. Nusselt number is directly proportional to the temperature slip parameter, concentration slip parameter and Prandtl number; and is inversely proportional to magnetic, radiation, Brownian movement and thermophoretic parameters. Similarly, Sherwood number is directly proportional to concentration slip, Brownian movement and Prandtl number; and it shows opposite behavior for magnetic, radiation, Brownian movement and thermophoretic parameters. Table 4 represents numerical values of Nusselt number for different values of the flow pertinent parameters in the presence linear and nonlinear thermal radiation parameter. The influence of all parameters on Nusselt number is similar to our observations as in Table 3. Further, it is interesting to note that, for all parameters, rate of heat transfer is more in the presence of nonlinear thermal radiation when compare to linear thermal radiation.

5. Conclusions

The main results of this study provided information regarding the velocity, temperature and concentration distribution of Prandtl nanofluid. Finally, based on the present study we have some important observations;

- Velocity temperature and concentration distributions and its layer thickness have same behavior for elastic parameter and Prandtl parameter.
- The increment in magnetic parameter corresponds to lesser thickness of momentum layer.
- The enhancement in temperature ratio and radiative parameters leads to larger temperature.
- Thermal and concentration slip parameters decrease the thicknesses of temperature and concentration boundary layers.
- Larger values of Nb and Nt temperature of fluid increases.
- Nonlinear thermal radiation is more effective when compare to liner thermal radiation.

References

[1] S. U. S. Choi and J. A. Eastman, “Enhancing thermal conductivity of fluids with nanoparticles”, *Proceedings of the ASME Int. Mech. Eng. Congress and Exposition*, Vol. 66, pp. 99-105, (1995).

[2] J. Buongiorno, “Convective transport in nanofluids”, *ASME J. Heat. Trans.*, Vol. 128, No. 3, pp. 240-250, (2005).

[3] W. A. Khan and I. Pop, “Boundary-layer flow of a nanofluid past a stretching sheet”, *Int.J. Heat and Mass Transfer*, Vol. 53, No. 11-12, pp. 2477-2483, (2010).

[4] O. D. Makinde, W. A. Khan and Z. H. Khan, “Buoyancy effects on MHD stagnation point flow and heat transfer of a nanofluid past a convectively heated stretching/shrinking sheet”, *Int. J. of Heat and Mass Transfer*, Vol. 6, No. 2, pp. 526-533, (2013).

[5] M. Sheikholeslami, S. Abelman and D. D. Ganji, “Numerical simulation of MHD nanofluid flow and heat transfer considering viscous dissipation”, *Int. J. Heat Mass Transfer*, Vol. 79, pp. 212-222, (2014).

[6] G. K. Ramesh, “Numerical study of the influence of heat source on stagnation point flow towards a stretching surface of a Jeffrey nanoliquid”, *Journal of Engineering*. Vol. 2015, 10 pages, (2015).

[7] G. K. Ramesh, S. A. Shehzad, T. Hayat and A. Alsaedi, “Activation energy and chemical reaction in Maxwell magneto-nanoliquid with passive control of nanoparticle volume fraction”, *Journal of the Brazilian Society of Mechanical Sciences and Engineering*, Vol. 40, pp. 422, (2018).

[8] B. J. Gireesha, K. Ganesh Kumar, G. K. Ramesh, and B. C. Prasannakumara, “Nonlinear convective heat and mass transfer of Oldroyd-B nanofluid over a stretching sheet in the presence of uniform heat source/sink”, *Results in Physics*, Vol. 9, pp. 1555-1563, (2018).

[9] K. Govardhan, G. Nagaraju, K. Kaladhar and M. Balasiddulu, “MHD and radiation effects on mixed convection unsteady flow of micropolar fluid over a stretching sheet”, *Procedia Comp. Sci.*, Vol. 57, pp. 65-76, (2015).

[10] R. Cortell, “A note on magnetohydrodynamic flow of a power-law fluid over a stretching sheet”, *Appl. Math. Comput*. Vol. 168, pp. 557-566, (2005).

[11] M. Y. Malik, T. Salahuddin, A. Hussain and S. Bilal, “MHD flow of tangent hyperbolic fluid over a stretching cylinder: Using Keller box method”, *J. of Magnetism and Magnetic Materials*, Vol. 395, pp. 271-276, (2015).

[12] R. Nasrin, S. Parvin and M. A. Alim, "Prandtl number effect on assisted convective heat transfer through a solar collector", *Applications and Applied Mathematics: An Int. J.,* Vol. 2, pp. 22-36, (2016).

[13] N. S. Akbar, S. Nadeem, R. Ul Haq and Z. H. Khan, "Numerical solutions of Magneto hydrodynamic boundary layer flow of tangent hyperbolic fluid flow towards a stretching sheet with magnetic field", *Indian J. Phys.,* Vol. 87, No. 11, pp. 1121-1124, (2013).

[14] R. Nasrin and M. A. Alim, "Prandtl number effect on free convective flow in a solar collector utilizing nanofluid", *Engg. Transac*., Vol. 7, No. 2, pp. 62-72, (2012).

[15] S. Nadeem, S. Ijaz and N. S. Akbar, "Nanoparticle analysis for blood flow of Prandtl fluid model with stenosis", *Int. Nano Letters,* Vol. 3, No. 35, pp. 2-13, (2013).

[16] S. A. Shehzad, T. Hayat, A. Alsaedi and A. O. Mustafa, "Nonlinear thermal radiation in three-dimensional flow of Jeffrey nanofluid: A model for solar energy", *Appl. Math. And Compu.*, Vol. 248, pp. 273-286, (2014).

[17] A. Zaib, M. M. Rashidi, A. J. Chamkha and N. F. Mohammad, "Impact of nonlinear thermal radiation on stagnation-point flow of a Carreau nanofluid past a nonlinear stretching sheet with binary chemical reaction and activation energy", *Proceedings of the Institution of Mechanical Engineers, Part C: Journal of Mechanical Engineering Science*. Vol. 232, No. 6, pp. 962-972, (2017).

[18] T. Hayat, S. Qayyum, A. Alsaedi and S. A. Shehzad, "Nonlinear thermal radiation aspects in stagnation point flow of tangent hyperbolic nanofluid with double diffusive convection", *Journal of Molecular Liquids,* Vol. 223, pp. 969-978, (2016).

[19] T. Hayat, T. Muhammad, A. Alsaedi and M.S. Alhuthali, "Magnetohydrodynamic three-dimensional flow of viscoelastic nanofluid in the presence of nonlinear thermal radiation", *J. Magnetism and Magnetic Materials*, Vol. 385, pp. 222-229, (2015).

[20] G. K. Ramesh and B. J. Gireesha, "Flow over a stretching sheet in a dusty fluid with radiation effect", *ASME J. Heat transfer*, Vol. 135, No. 10, pp. 102702 (1-6), (2013).

[21] M. Mustafa, A. Mushtaq, T. Hayat,and A. Alsaedi, "Numerical study of the non-linear radiation heat transfer problem for the flow of a second-grade fluid", *J. Bulgarian Chemi. Commun.,* Vol. 47, No. 2, pp. 725-732, (2015).

[22] G. K. Ramesh, A. J. Chamkha and B. J. Gireesha, "Boundary layer flow past an inclined stationary/moving flat plate with convective boundary condition", *Afrika Matematika*, Vol. 27. No. 1-2, pp. 87-95, (2016).

[23] C. Y. Wang, "Flow due to a stretching boundary with partial slip an exact solution of the Navier-Stokes equations", *Chem. Eng. Sci*., Vol. 57, pp. 3745-3747, (2002).

[24] S. Mukhopadhyay and R. S. R. Gorla, "Effects of partial slip on boundary layer flow past a permeable exponential stretching sheet in presence of thermal radiation". *Heat Mass Trans.*, Vol. 45, pp. 1447-1452, (2009).

[25] T. Fang, S. Yao, J. Zhang and A. Aziz, "Viscous flow over a shrinking sheet with a second order slip flow model". *Commun. Nonlinear Sci. and Numerical Simul*., Vol. 15, No. 7, pp. 1831-1842, (2010).

[26] K. Bhattacharyya, S. Mukhopadhyay and G. C Layek, "Slip effects on boundary layer stagnation-point flow and heat transfer towards a shrinking sheet", *Int. J. Heat and Mass Tran*., Vol. 54, No. 1-3, pp. 308-313, (2011).

[27] S. Das, R. N. Jana and O. D. Makinde, "MHD boundary layer slip flow and heat transfer of nanofluid past a vertical stretching sheet with non-uniform heat generation/absorption". *Int. J. Nanosci*., Vol. 13, No. 3, 1450019, (2014).

[28] M. Kezzar and M. Rafik Sari, "Series solution of nanofluid flow and heat transfer between stretchable/shrinkable inclined walls", *International Journal of Applied and Computational Mathematics*, Vol. 3, No. 3, pp. 2231-2255, (2017).

[29] M. Kezzar, M. Rafik Sari, R. Bourenane, M. M. Rashidi and A. Haiahem, "Heat transfer in hydro-magnetic nano-fluid flow between non parallel plates using DTM", (2018). DOI: 10.22055/JACM.2018.24959.1221

[30] C. Y. Wang, "Free convection on a vertical stretching surface", *J. Appl. Math. Mech.* (ZAMM), Vol. 69, pp. 418-420, (1989).

[31] R. S. R. Gorla and I. Sidawi, "Free convection on a vertical stretching surface with suction and blowing", *Appl. Sci. Res.*, Vol. 52, pp. 247-257, (1994).

How to cite this paper:

K. Ganesh Kumar, G. K. Ramesh, S. A. Shehzad and B. J. Gireesha, "Magneto Prandtl nanofluid past a stretching surface with non-linear radiation and chemical reaction", *Journal of Computational and Applied Research in Mechanical Engineering,* Vol. 9, No. 2, pp. 275-285, (2019).

DOI: 10.22061/jcarme.2018.3180.1350

URL: http://jcarme.sru.ac.ir/?_action=showPDF&article=906